Correlated Gaussian hyperspherical method for few-body systems

Javier von Stecher and Chris H. Greene
Department of Physics and JILA, University of Colorado, Boulder, Colorado 80309-0440, USA
(Received 8 April 2009; published 11 August 2009)

We develop a numerical technique to describe few-body systems. Correlated Gaussian basis functions are used to expand the channel functions in the hyperspherical representation. The method is proven to be robust and efficient compared to other numerical techniques. The method is applied to few-body systems with short-range interactions, including several examples for three- and four-body systems. Specifically, for the two-component, four-fermion system, we extract the coefficients that characterize its behavior at unitarity.

DOI: 10.1103/PhysRevA.80.022504 PACS number(s): 31.15.xj, 34.50.Cx

I. INTRODUCTION

Ultracold gases in traps or optical lattices have opened new possibilities in the study of strongly correlated quantum systems. From the rich few-body physics of the Efimov effect [1–4] to the fascinating many-body physics of the BCS-Bose Einstein condensate (BEC) crossover [5–14], experimentalists are now able to realize a wide variety of physical systems of great interest for the atomic, nuclear, and condensed-matter communities. In particular, the pureness and controllability of cold atoms in optical lattices [15–17] make them perfect candidates for the experimental implementation of condensed-matter models [see Ref. [18] and references therein]. In all these systems, the rich physics that governs a few interacting atoms is crucial for understanding recent experiments.

For that reason, extensive efforts have concentrated on the development of an accurate description of few-body systems. Encouraging advances have been achieved in the last decade in the understanding ultracold three-body problem [1,3,19,20]. These studies have demonstrated the importance of three-body recombination and relaxation processes and have determined the effective interaction in atom-dimer collisions. Some of these techniques were subsequently extended to four-body systems [21–25] in a few applications. However, the physics of the four-body problem are far richer and more complicated. Also, it is a very challenging numerical problem and for that reason, it has remained largely unsolved except in very limited regimes. Here, we present a numerical method to handle few-body systems that can be used to efficiently describe four-body systems, through a combination of different techniques.

Even though several techniques have been developed in recent decades to provide solutions for few-body systems [26–30], not many of them have been applied to numerically solve the Schrödinger equation for systems with more than three particles. Among these methods, the correlated Gaussian (CG) technique [31–37] in particular has proven to be capable of describing a trapped few-body system with short-range interactions. Because of the simplicity of the matrix-element calculation, the CG method provides an accurate description of the ground and excited states up to $N_P=6$ particles [35,36,38]. However, the CG method as originally implemented can only describe bound states. For this reason, previous studies have focused on trapped systems where all the eigenstates are discrete [23,38–40]. In fact, the CG method requires a nontrivial extension in order to describe the continuum and the rich behavior of atomic collisions, such as dissociation, rearrangement, and recombination processes. Some progress on this direction was achieved in a series of studies [41–44]. Here, we propose an alternative approach.

The hyperspherical representation, in fact, provides an appropriate framework that can treat the continuum [30,45–49]. In the adiabatic hyperspherical representation, the Hamiltonian is diagonalized as a function of the hyperradius R, reducing the Schrödinger equation to a set of coupled equations in a single variable, with a series of different effective potentials and couplings. The asymptotic behavior of the channel potentials describes different dissociation or fragmentation pathways and provides a suitable framework for analyzing collision physics. These solutions can be readily combined with scattering methods such as the R-matrix approach [50–52] to provide an accurate description of the collisional dynamics. However, the standard hyperspherical methods expand the hyperangular channel functions in a B spline or finite element basis set [53–56] and the calculations become very computationally demanding for $N_P>3$ systems.

It is therefore natural to combine the scalability of the CG method with the advantages of the hyperspherical representation. In this paper, we present a way to achieve this combination in what we term the correlated Gaussian hyperspherical (CGHS) method. This method uses CG basis functions to expand the channel functions in the hyperspherical representation. We show that also in this case, the matrix-element evaluation is greatly simplified thanks to the simple form of the CG basis functions. Furthermore, thanks to the explicit correlation incorporated in these basis functions, only a relatively small basis set is needed to achieve convergence of the lowest channel functions even in the strongly interacting regime.

To illustrate the power of the CGHS method, we carry out calculations for $N_P=3,4$-particle systems in the strongly interacting regime. First, we analyze systems of three bosons or three fermions at unitarity and show that the method recovers results that agree with semianalytical predictions. Then, we consider the two-component four-fermion system, in the large and positive scattering length regime, and reproduce the lowest potential curves from Ref. [24]. The CGHS provides a larger number of channels which would allow the

calculation of scattering events not considered in Ref. [24]. Finally, we focus on the universal behavior of four fermions at unitarity. In this regime, the energies of the trapped system are trivially determined by the hyperspherical potential curves [38,57]. Therefore, we can compare our calculations to predictions for the trapped system [23,58–61]. Our results improve and extend these previous predictions and characterize the 20 lowest potential curves for even parity and vanishing orbital angular momentum.

This paper continues as follows. First, we review both the CG and hyperspherical methods in Sec. II. In Sec. III, we introduce the main idea of the CGHS method, leaving some details of the implementation for the Appendix A. Section IV presents our results for three-body systems and for the four-fermion system. Finally, Sec. V presents our conclusions.

II. THEORETICAL BACKGROUND

This section discusses the general form of the Hamiltonian that we are trying to diagonalize and, in Sec. II A, reviews the correlated Gaussian method. Section II B presents the general formalism of the hyperspherical representation and describes how to numerically solve the Schrödinger equation in this representation using a correlated Gaussian basis set expansion.

The methods described in this paper solve the time-independent Schrödinger equation for a Hamiltonian of the form

$$H = \sum_i \left(\frac{-\hbar^2}{2m_i} \nabla_i^2 + V_{ext}(\mathbf{r}_i) \right) + \sum_{i,j} V_0(r_{ij}), \tag{1}$$

where V_{ext} is an external trapping potential and V_0 is the interaction potential. The form of the Hamiltonian can be varied depending on the particular problem we are considering. In the CG method, one will usually consider a spherically symmetric harmonic trapping potential $V_{ext}(\mathbf{r}) = \frac{1}{2} m_i \omega^2 \mathbf{r}_i^2$ but in hyperspherical calculations we usually consider a free system ($V_{ext}(\mathbf{r})=0$). We can always include the harmonic trapping potential in the final step of the hyperspherical calculation, since it is a purely hyperradial potential. Depending on the symmetry properties of the particles considered, the interaction term will change. For example, all particles interact with each other in identical boson systems but only opposite-spin fermions interact in two-component Fermi systems (except in a few problems involving p-wave Fano-Feshbach resonances). Also, in many cases, the center-of-mass motion decouples from the more interesting internal degrees of freedom and it is preferable to use a set of Jacobi coordinates rather than the usual single-particle coordinates. All such options can be treated using the method presented below.

A. Correlated Gaussian method

Different types of Gaussian basis functions have long been used in many different areas of physics. In particular, the usage of Gaussian basis functions is one of the key elements of the success of *ab initio* calculations in quantum chemistry. The idea of using an explicitly correlated Gaussian to solve quantum chemistry problems was introduced in 1960 by Boys [32] and Singer [31]. The combination of a Gaussian basis and the stochastical variational method (SVM) was first introduced by Kukulin and Krasnopol'sky [33] in nuclear physics and was extensively used by Varga and Suzuki [34–37]. These methods were also used to treat ultracold many-body Bose systems by Sorensen *et al.* [62]. A detailed discussion of both the SVM and CG methods can be found in a thesis of Sorensen [63] and, in particular, in the book by Suzuki and Varga [27]. In the following, we highlight the main ideas of the CG method.

Consider a set of coordinate vectors that describe the system $\{\mathbf{x}_1, \ldots, \mathbf{x}_N\}$. In this method, the eigenstates are expanded in a set of basis functions

$$\Psi(\mathbf{x}_1, \ldots, \mathbf{x}_N) = \sum_A C_A \Phi_A(\mathbf{x}_1, \ldots, \mathbf{x}_N). \tag{2}$$

Here, A specifies a matrix with a particular set of parameters that characterize the basis function. It is convenient to introduce the following ket notation, $\Phi_A(\mathbf{x}_1, \ldots, \mathbf{x}_N) = \langle \mathbf{x}_1, \ldots, \mathbf{x}_N | A \rangle$. The solution of the time-independent Schrödinger equation in this basis set reduces the problem to one of diagonalizing the Hamiltonian matrix

$$\mathcal{H} \vec{C}_i = E_i \mathcal{O} \vec{C}_i. \tag{3}$$

Here, E_i are the energies of the eigenstates, $\vec{C}_i$ is a vector formed with the coefficients C_A and $\mathcal{H}$, and $\mathcal{O}$ are matrices whose elements are $\mathcal{H}_{BA} = \langle B | \mathcal{H} | A \rangle$ and $\mathcal{O}_{BA} = \langle B | A \rangle$. For a three-dimensional (3D) system, the evaluation of these matrix elements involves $3N$-dimensional integrations which are in general very expensive to compute. Therefore, the effectiveness of the basis set expansion method relies mainly on the appropriate selection of the basis functions. As we will see, the CG basis functions permit fast evaluation of overlap and Hamiltonian matrix elements and they are flexible enough to correctly describe physical states.

To reduce the dimensionality of the problem, we can take advantage of its symmetry properties. Since the interactions considered are spherically symmetric, the total angular momentum, L, is a good quantum number. For simplicity, we will restrict ourselves to $L=0$ solutions. This restriction allows us to reduce the Hilbert space by introducing restrictions on the basis functions. In particular, if the basis functions only depend on the interparticle distances, then Eq. (2) can only describe states with zero angular momentum and positive parity ($L^P = 0^+$). Furthermore, we can recognize that the center-of-mass motion decouples from the system. In such cases, the CG basis functions take the form

$$\Phi_A(\mathbf{x}_1, \ldots, \mathbf{x}_N) = \psi_0(\mathbf{R}_{CM}) \mathcal{S} \left\{ \exp\left(- \sum_{j>i=1}^{N} \alpha_{ij} r_{ij}^2 / 2 \right) \right\}, \tag{4}$$

where $\mathcal{S}$ is a symmetrization operator and r_{ij} is the interparticle distance between particles i and j. Here, ψ_0 is the ground state of the center-of-mass motion. For trapped systems, ψ_0 takes the form $\psi_0(\mathbf{R}_{CM}) = e^{-R_{CM}^2/2(a_{ho}^M)^2}$. Because of its simple Gaussian form, ψ_0 can be absorbed in the expo-

nential factor. Thus, in a more general way, the basis function can be written in terms of a matrix A that characterizes them

$$\Phi_A(\mathbf{x}_1,\mathbf{x}_2,\ldots,\mathbf{x}_N) = \mathcal{S}\left\{\exp\left(-\frac{1}{2}\mathbf{x}^T\cdot A\cdot\mathbf{x}\right)\right\} = \mathcal{S}\left\{\exp\left(-\frac{1}{2}\sum_{j,i=1}^{N} A_{ij}\mathbf{x}_i\cdot\mathbf{x}_j\right)\right\}, \quad (5)$$

where $\mathbf{x}=\{\mathbf{x}_1,\mathbf{x}_2,\ldots,\mathbf{x}_N\}$ and A is a symmetric matrix. The matrix elements $A_{ij}=A_{ji}$ can be expressed in terms of the α_{ij}. Because of the simplicity of the basis functions, Eq. (4), the matrix elements of the Hamiltonian can be calculated analytically.

The analytical evaluation of the matrix elements is enabled by selecting the set of coordinates that simplifies the evaluations. For basis functions of the form of Eq. (5), the matrix elements are characterized by a matrix M in the exponential. Then, the matrix-element integrand greatly simplifies if we rewrite it in terms of the coordinate vectors that diagonalize that matrix M. This change of coordinates permits, in many cases, the analytical evaluation of the matrix elements. The explicit evaluation of several matrix elements can be found in Refs. [27,63].

In general, we need to include the spin part of the wave function for the description of the system. However, for the bosonic and fermionic systems considered in this paper, the spin part can be decoupled from the spatial part. In the case of a two-component Fermi system, we adopt a standard approximation and we assume that we can treat different components as consisting of distinguishable particles. Therefore, all the statistical information of the system is conveyed in the appropriate selection of the symmetrization operator $\mathcal{S}$.

Two properties of the CG method deserve mentioning at this point. First, the CG method does not rely on any approximation other than basis set truncation and the solutions can be systematically improved. The accuracy of the results is only limited by numerical issues related to linear dependence of the basis set. Second, the basis functions Φ_A are square integrable only if the matrix A is positive definite. This ensures that the wave function decays in all degrees of freedom. We can further restrict the basis functions by introducing real widths d_{ij} such that $\alpha_{ij}=1/d_{ij}^2$. With this transformation, we ensure that A is positive definite. Furthermore, each such width is proportional to the mean interparticle distances covered by that basis function. Thus, it is relatively easy to select the widths after considering the physical length scales relevant to the problem. Even though we have restricted the Hilbert space with this transformation, we have numerical evidence that the results converge to the exact eigenvalues.

The linear dependence in the basis set causes problems in the numerical diagonalization of the Hamiltonian matrix, Eq. (3). To minimize these linear dependence problems, we restrict the basis function so that the overlap between any two normalized basis functions is below some cutoff value. The other method we use to eliminate linear dependence applies a linear transformation to produce a smaller orthonormal basis set.

Finally, we stress the importance of making an appropriate selection of the interaction potential. For the problems considered in this paper, the interactions are expected to be characterized only by the scattering length, i.e., to be independent of the shape of the potential. For that reason, we can select a model potential that permits rapid evaluation of the matrix elements. We have found that a model potential with a Gaussian form,

$$V_0(r) = -V_0\exp\left(-\frac{r^2}{2r_0^2}\right), \quad (6)$$

is particularly suitable for this basis set expansion since it can be absorbed in the exponential form of the wave functions for matrix-element evaluation. If the range r_0 is much smaller than the scattering length, then the interactions are effectively characterized only by the scattering length. The scattering length is tuned by changing the strength of the interaction potential, V_0, while the range, r_0, of the interaction potential remains unchanged. This is particularly convenient in this method since it implies that we only need to evaluate the matrix elements once and we can use them to solve the Schrödinger equation at any given potential strength (or scattering length). Of course, this procedure will give accurate results only if the basis set is sufficiently flexible and complete to describe the different configurations that appear at different scattering lengths.

In general, this method includes five basic steps: generation of the basis set, evaluation of the matrix elements, elimination of linear dependence, evaluation of the eigenvalue spectrum, followed by a study of stability and convergence. The SVM of Refs. [27,63] combines the first three of these steps in an optimization procedure where the basis functions are selected randomly.

B. Hyperspherical representation

The main objective of the hyperspherical method is to solve the time-independent Schrödinger equation in a convenient and efficient way that also provides insight into the relevant reaction pathways by which various collision processes can occur. The first step involves calculation of eigenvalues and eigenfunctions of the fixed-hyperradius Hamiltonian, which defines the adiabatic hyperspherical representation. These eigenvalues and eigenfunctions are then used to construct a set of one-dimensional (1D) coupled equations in the hyperradius R. The hyperradius is a collective coordinate related to the total moment of inertia of the system [48,64]. In a system described by N coordinate vectors $\mathbf{r}_1,\ldots,\mathbf{r}_N$, the hyperradius R is defined by

$$\mu R^2 = \sum_{i=1}^{N} m_i\mathbf{r}_i^2. \quad (7)$$

Here, μ is an arbitrary mass factor called the hyperradial reduced mass [65] and m_i are the Jacobi masses corresponding to the Jacobi vector i. The remaining coordinates are described by a set of hyperangles collectively denoted as Ω.

The total number of spatial dimensions of this N-vector system is $d=3N$. The total wave function ψ is rescaled by R, $\Psi=R^{(d-1)/2}\psi$, so that the hyperradial equation resembles a coupled one-dimensional Schrödinger equation. In the adiabatic representation, the wave function $\Psi_E(R,\Omega)$ is expanded in terms of a complete orthonormal set of angular wave functions Φ_ν and radial-wave functions $F_{\nu E}$, such that

$$\Psi_E(R,\Omega)=\sum_\nu F_{\nu E}(R)\Phi_\nu(R;\Omega). \tag{8}$$

The adiabatic eigenfunctions, or channel functions Φ_ν, depend parametrically on R and are eigenfunctions of a $3N-1$ partial differential equation (which corresponds to $3N_P-4$ dimensions since the center-of-mass motion is removed explicitly)

$$\left(\frac{\hbar^2\Lambda^2}{2\mu R^2}+\frac{(d-1)(d-3)\hbar^2}{8\mu R^2}+V(R,\Omega)\right)\Phi_\nu(R;\Omega) = U_\nu(R)\Phi_\nu(R;\Omega). \tag{9}$$

Here, Λ is the grand angular-momentum operator, which is related to the kinetic term by

$$-\sum_i\frac{\hbar^2\nabla_i^2}{2m_i}=-\frac{\hbar^2}{2\mu}\frac{1}{R^{d-1}}\frac{\partial}{\partial R}R^{d-1}\frac{\partial}{\partial R}+\frac{\Lambda^2\hbar^2}{2\mu R^2}. \tag{10}$$

The $U_\nu(R)$ obtained in Eq. (9) are effective hyperradial potential curves that appear in a set of coupled one-dimensional differential equations

$$\left[-\frac{\hbar^2}{2\mu}\frac{d^2}{dR^2}+U_\nu(R)\right]F_{\nu E}(R)-\frac{\hbar^2}{2\mu}\sum_{\nu'}\left[2P_{\nu\nu'}(R)\frac{d}{dR}+Q_{\nu\nu'}(R)\right]F_{\nu' E}(R)=EF_{\nu E}(R). \tag{11}$$

These differential equations [Eq. (11)] are coupled through the $P_{\nu\nu'}(R)$ and $Q_{\nu\nu'}(R)$ couplings defined as

$$P_{\nu\nu'}(R)=\langle\Phi_\nu(R;\Omega)|\frac{\partial}{\partial R}|\Phi_{\nu'}(R;\Omega)\rangle|_R, \tag{12}$$

$$Q_{\nu\nu'}(R)=\langle\Phi_\nu(R;\Omega)|\frac{\partial^2}{\partial R^2}|\Phi_{\nu'}(R;\Omega)\rangle|_R. \tag{13}$$

Since the basis set expansion of the wave function, Eq. (8), is complete in the $3N$-dimensional space, Eqs. (9) and (11) reproduce exactly the original d-dimensional Schrödinger equation. As in most numerical methods, the solutions are approximated by truncating the Hilbert space. In this case, the Hilbert space is truncated by considering a finite number of channels in Eq. (11). This approximation is easily tested by analyzing convergence with respect to the number of channels included in the calculation.

The utility of the hyperspherical representation relies on the assumption that the wave-function variation with the hyperradius R is smooth. In such cases, only a few channels are relevant and the couplings are small and vary smoothly with R. Furthermore, a fairly good approximation to the solutions can be achieved by truncating the expansion in Eq. (8) to a single term

$$\Psi_E(R,\Omega)=F_{\nu E}(R)\Phi_\nu(R;\Omega). \tag{14}$$

This adiabatic hyperspherical approximation leads to an effective one-dimensional Schrödinger equation

$$\left[-\frac{\hbar^2}{2\mu}\frac{d^2}{dR^2}+W_\nu(R)\right]F_{\nu E}(R)=EF_{\nu E}(R), \tag{15}$$

where the effective potential is

$$W_\nu(R)=U_\nu(R)-\frac{\hbar^2}{2\mu}Q_{\nu\nu}(R). \tag{16}$$

Here, the first term is the hyperradial potential curve and the second term is "adiabatic correction," i.e., the repulsive kinetic contribution of the hyperradial dependence of the channel function. If the potential curves are well separated and have no strong avoided crossings in the relevant range of energy and radius, then the adiabatic approximation can be quite accurate for the lower states in any given potential curve. This approximation comes from a truncation of the Hilbert space and, for that reason, obeys the variational principle. Any discrete energy eigenvalue obtained with this method is an upper bound of the exact energy level in the sense of the Hylleraas-Undheim theorem. An approximate description of the spectrum can be achieved by combining the energies obtained from the adiabatic approximation applied to each channel separately. For example, bound states of excited potential curves which are above the lowest fragmentation threshold would represent quasibound states. This approach is equivalent to neglecting all off-diagonal couplings in Eq. (11) and produces an approximate spectrum which is not variational. Another useful approximation is obtained by neglecting the second term in Eq. (16), i.e., replacing $W_0(R)$ by $U_0(R)$ in Eq. (15). This is usually called the hyperspherical Born-Oppenheimer approximation. As in the standard Born-Oppenheimer approximation for a diatomic molecule, the approximate energy obtained in this manner represents a lower bound to the exact ground-state energy [66]. Next, we show how Eq. (9) is solved and how the $P_{\nu\nu'}$ and $Q_{\nu\nu'}$ are evaluated.

C. Expansion of the channel function in a basis set

In the hyperspherical method (see Sec. II B), channel functions are eigenfunctions of the adiabatic Hamiltonian $\mathcal{H}_A(R;\Omega)$,

$$\mathcal{H}_A(R;\Omega)\Phi_\nu(R;\Omega)=U_\nu(R)\Phi_\nu(R;\Omega). \tag{17}$$

The eigenvalues of this equation are the hyperspherical potential curves $U_\nu(R)$, which serve as readily visualizable reaction pathways. The adiabatic Hamiltonian has the form

$$\mathcal{H}_A(R;\Omega)=\frac{\hbar^2\Lambda^2}{2\mu R^2}+\frac{(d-1)(d-3)\hbar^2}{8\mu R^2}+V(R,\Omega). \tag{18}$$

A standard way to solve Eq. (17) is to expand the channel functions in a basis,

$$|\Phi_\mu(R;\Omega)\rangle = \sum_i |B_i(R;\Omega)\rangle c_{i\mu}(R). \tag{19}$$

Here, μ labels the channel function. The $|B_i(R;\Omega)\rangle$ are the basis functions. With this expansion, Eq. (17) reduces to the eigenvalue equation

$$\mathcal{H}_A(R)\vec{c}_\mu = U_\mu(R)\mathcal{O}(R)\vec{c}_\mu. \tag{20}$$

The μth column vector $\vec{c}_\mu = \{c_{i\mu}\}, i=1,\ldots,D$, where D is the dimension of the basis set. $\mathcal{H}_A$ and $\mathcal{O}$ are the Hamiltonian and overlap matrices whose matrix elements are given by

$$\mathcal{H}_A(R)_{ij} = \langle B_i|\mathcal{H}_A(R;\Omega)|B_j\rangle|_R, \tag{21}$$

$$\mathcal{O}(R)_{ij} = \langle B_i|B_j\rangle|_R. \tag{22}$$

Once the hyperradial potential curves are calculated, we still need to evaluate the P and Q nonadiabatic couplings between the channel functions [Eq. (12) in Sec. II B]. To evaluate the Q coupling, we use the identity

$$Q_{\nu\mu}(R) = -\widetilde{Q}_{\nu\mu}(R) + \frac{\partial P_{\nu\mu}(R)}{\partial R}, \tag{23}$$

where

$$\widetilde{Q}_{\nu\mu} = \left\langle \frac{\partial}{\partial R}\Phi_\nu(R)\middle|\frac{\partial}{\partial R}\Phi_\mu(R)\right\rangle. \tag{24}$$

Thus, we can obtain all the couplings from the evaluation of P and $\widetilde{Q}$. In the basis set expansion, P and $\widetilde{Q}$ can be calculated using matrix multiplication. With the expansion in Eq. (19),

$$|\dot{\Phi}_\mu(R)\rangle = \sum_i |B_i\rangle\dot{c}_{i\mu} + |\dot{B}_i\rangle c_{i\mu}. \tag{25}$$

Here and in the following, we have omitted the radial and angular dependences of functions and we have introduced the notation $\dot{F}$ for the derivative of F with respect to R. The P coupling takes the form

$$P_{\nu\mu} = \sum_{ij} c^T_{\nu j}\langle B_j|B_i\rangle\dot{c}_{i\mu} + c^T_{\nu j}\langle B_j|\dot{B}_i\rangle c_{i\mu} = \vec{c}^T_\nu\mathcal{O}\dot{\vec{c}}_\mu + \vec{c}^T_\nu\mathcal{P}\vec{c}_\mu, \tag{26}$$

where $\mathcal{P}(R)$ is defined later in Eq. (29). The same procedure can be done for the $\widetilde{Q}$ matrix elements with

$$\widetilde{Q}_{\nu\mu} = \sum_{ij} \dot{c}^T_{\nu j}\langle B_j|B_i\rangle\dot{c}_{i\mu} + \dot{c}^T_{\nu j}\langle B_j|\dot{B}_i\rangle c_{i\mu} + c^T_{\nu j}\langle\dot{B}_j|B_i\rangle\dot{c}_{i\mu} + c^T_{\nu j}\langle\dot{B}_j|\dot{B}_i\rangle c_{i\mu} \tag{27}$$

and can also be written in terms of matrix multiplications

$$\widetilde{Q}_{\nu\mu} = \dot{\vec{c}}^T_\nu\mathcal{O}(R)\dot{\vec{c}}_\mu + \dot{\vec{c}}^T_\nu\mathcal{P}(R)\vec{c}_\mu + \vec{c}^T_\nu\mathcal{P}^T(R)\dot{\vec{c}}_\mu + \vec{c}^T_\nu\widetilde{\mathcal{Q}}(R)\vec{c}_\mu. \tag{28}$$

In Eqs. (26) and (28), we have used the overlap matrix $\mathcal{O}$ and defined the matrices $\mathcal{P}$ and $\widetilde{\mathcal{Q}}$ whose matrix elements are

$$\mathcal{P}(R)_{ij} = \langle B_i(R)|\dot{B}_j\rangle \quad \text{and} \quad \widetilde{\mathcal{Q}}(R)_{ij} = \langle\dot{B}_i|\dot{B}_j\rangle. \tag{29}$$

The derivatives of the $\dot{c}_{i\mu}(R)$ coefficients that form the $\dot{\vec{c}}_\mu$ are calculated numerically using the three-point rule.

III. CORRELATED GAUSSIAN HYPERSPHERICAL METHOD

As we have seen in the previous section, the implementation of hyperspherical calculations requires the evaluation of the Hamiltonian matrix elements at fixed R [Eqs. (21) and (22)]. This is one of most time-consuming part of the calculation which for an $N_P=4$ system requires a five–dimensional (5D) integration. Thus, we need to find an efficient way to evaluate Hamiltonian matrix elements at fixed R. As a prelude, we first review how multidimensional matrix-element evaluations reduce to analytical forms in the standard CG method. This will be the key to evaluating matrix elements in the hyperspherical variant of this method.

In the CG method, we select, for each matrix-element evaluation, a set of coordinate vectors that simplifies the integration, i.e., the set of coordinate vectors that diagonalize the basis matrix M which characterizes the matrix element. The flexibility to choose the best set of coordinate vectors for each matrix-element evaluation is crucial for the economy of the CG method.

This selection of the optimal set of coordinate vectors is formally applied by an orthogonal transformation from an initial set of vectors $\mathbf{x}=\{\mathbf{x}_1,\ldots,\mathbf{x}_N\}$ to a final set of vectors $\mathbf{y}=\{\mathbf{y}_1,\ldots,\mathbf{y}_N\}$: $T\mathbf{x}=\mathbf{y}$, where T is the orthogonal transformation matrix. The hyperspherical method is particularly suitable for such orthogonal transformations because the hyperradius R is an invariant under them. Consider the hyperradius defined in terms of a set of mass-scaled Jacobi vectors [45,46,56,67], $\mathbf{x}=\{\mathbf{x}_1,\ldots,\mathbf{x}_N\}$,

$$\mu R^2 = \mu\sum_i \mathbf{x}_\mathbf{i}^2. \tag{30}$$

If we applied an orthogonal transformation to a new set of vectors $\mathbf{y}$, then

$$\mu R^2 = \mu\sum_i \mathbf{x}_\mathbf{i}^2 = \mu\mathbf{y}T^TT\mathbf{y} = \mu\sum_i \mathbf{y}_\mathbf{i}^2, \tag{31}$$

where we have used the fact that $T^TT=I$ and I is the identity. Therefore, in the hyperspherical framework, we can also select the most convenient set of coordinate vectors for each matrix-element evaluation. This will be the key to reducing the dimensionality of the matrix-element integration. This transformation amounts to selecting, for each matrix-element evaluation, the set of hyperangles (Ω) that simplify the matrix-element evaluation.

As an example of how the dimensionality of matrix-element integration is thereby reduced, consider an $L=0$ three-dimensional N_P-particle system with the center of mass removed. It can be shown that this technique reduces a $(3N_P-7)$ numerical integration [68] to a sum over the symmetrization permutation of (N_P-3) numerical integrations. This result implies that for $N_P=3$, the matrix-element evalu-

ation can be done analytically (see the Appendix A, Sec. A 1) and that for $N_P=4$, it requires a sum of one-dimensional numerical integrations [69].

Once the basic idea of the appropriate change of variables for each matrix-element calculation is understood, the actual calculation of the matrix elements using correlated Gaussian basis function is straightforward. Appendix A, Sec. A 1 shows, as an example, how the matrix elements can be calculated analytically for a three-particle system (the calculation of the matrix elements for $N_P=4$ are not presented here but can be found in Ref. [69]). Finally, Appendix A, Sec. A 2 discusses in general how this method is implemented.

IV. RESULTS

In this section, we present CGHS results for $N_P=3,4$. First, we analyze two different $N_P=3$ systems and compare them to analytical predictions. Then, we present four-fermion potential curves and compare them to recent predictions [24]. Finally, we characterize the four-fermion $L=0$ potential curves at unitarity and extract the s_ν coefficient that characterizes the universal regime.

To test the CGHS method, we calculate the hyperspherical potential curves at unitarity for three interacting bosons. For zero-range interactions, the potential curves at unitarity are inversely proportional to the hyperradius. For example, the lowest potential curve for three identical bosons is given by

$$U_0(R) = -\frac{s_0^2 + 1/4}{2\mu R^2}. \tag{32}$$

The coefficient $s_0 \approx 1.0062$ can be obtained analytically in the theory of Efimov states [1,2,70]. A simple and fast numerical CGHS calculation with only 30 basis functions extended up to $R=100r_0$ shows, at large R, the expected $1/R^2$ behavior. Extrapolation of our potential curves to $R\to\infty$ gives $s_0 \approx 1.0059$.

Similarly, we analyze the system of two indistinguishable fermions resonantly interacting with a third particle of equal mass. For such system, the zero-range model predicts a lowest potential of the form

$$U_0(R) = \frac{p_0^2 - 1/4}{2\mu R^2}. \tag{33}$$

The value of $p_0 \approx 2.166\,222$ can also be predicted analytically. Using a slightly larger basis set of 90 basis function, we extend the CGHS calculations up to $R=4000r_0$. Extrapolating our potential curves to $R\to\infty$, we obtain $p_0 \approx 2.166\,218$.

These two examples show that the CGHS method is flexible enough to describe a strongly interacting system with relatively small basis sets and analytical matrix-element evaluations. The main limitation of these calculations comes from linear dependence issues. At the $N_P=3$ level, this method cannot probably compete with more sophisticated calculations which permit calculations up to $R=10^6r_0$ [3,56]. However, it has been a challenge to extend hyperspherical methods beyond $N_P=3$. One successful method uses Monte Carlo techniques to describe the lowest channel function and extends it application to large ($N_P \lesssim 10$) systems [71]. However, this method can only calculate the lowest potential curve and leads to an approximate solution. In contrast, the CGHS method can be readily extended to $N_P=4$ particles (and possibly beyond) and allows to obtain a full solution which represents the current *state of the art* of hyperspherical methods.

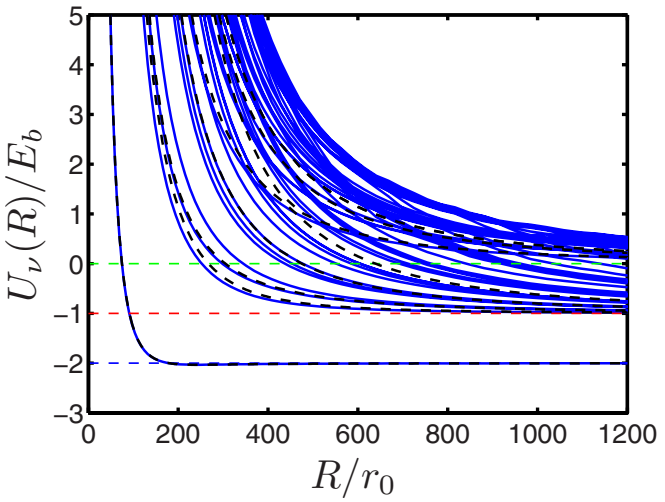

FIG. 1. (Color online) Adiabatic hyperspherical potential curves $U_\nu(R)$ (solid lines) for two spin-up and two spin-down fermions with an atom-atom scattering length $a_s=100r_0$. The dashed line at $E=2E_b$ (blue) is the dimer-dimer threshold, the dashed line at $E=E_b$ (red) is the dimer–two-atom threshold, and the dashed line at $E=0$ (green) is the four-atom threshold. Dashed curves are predictions from Ref. [24].

The development of four-body hyperspherical methods allows, for one thing, an analysis of the full energy dependence of the dimer-dimer scattering length. Figure 1 presents the four-fermion potential curves obtained with the CGHS method. There are three relevant energy thresholds marked with dashed lines in Fig. 1: dimer-dimer threshold at $2E_b$, dimer–two-atom threshold at E_b, and four-atom threshold at 0 energy. The lowest curve represents the dimer-dimer channel and potential curves going asymptotically to E_b and 0 represent dimer–two-atom and four-atom channels, respectively. Standard multichannel scattering techniques, such as the R-matrix method, can be applied to solve the hyperspherical coupled differential equations. This analysis was performed in a recent study by D'Incao *et al.* [24], which obtained the energy dependence of the dimer-dimer scattering length for equal-mass systems. Black dashed curves in Fig. 1 represent the potential curves of Ref. [24]. As we can see, the CGHS method presented here predicts very similar potential curves. The dimer-dimer potential curves obtained with the different methods are almost indistinguishable. For dimer–two-atom potential curves, the CGHS predicts lower potential curves suggesting that the CGHS calculation is slightly better. At large R, the asymptotic behaviors of both methods agree. This is very encouraging since in the method of D'Incao *et al.*, the asymptotic behavior of the channel functions is correct by construction, whereas in the CGHS it constitutes an important, nontrivial test. Preliminary calculations with the CGHS potential curves predict a similar en-

TABLE I. Noninteracting coefficients p_ν^{NI} of the four-fermion potential curves and their degeneracies λ_ν.

ν	p_ν^{NI}	λ_ν	ν	p_ν^{NI}	λ_ν
0	11/2	1	5	31/2	50
1	15/2	3	6	35/2	80
2	19/2	8	7	39/2	120
3	23/2	16	8	43/2	175
4	27/2	30	9	47/2	245

ergy dependence of the dimer-dimer scattering length. Therefore, the CGHS opens the possibility for accurately analyzing four-body scattering events, as has been carried out for four interacting bosons in Refs. [72,73].

The calculations of the potential curves at unitarity allow us to extract the four-fermion universal coefficients. As in the $N_P=3$ system, the potential curves can be written as [57,74]

$$U_\nu(R) = \frac{p_\nu^2 - 1/4}{2\mu R^2}. \tag{34}$$

This functional form of the potential curves was verified indirectly in Ref. [38] by analyzing the spectrum of the four-fermion system under spherical harmonic confinement. It can be shown that all the couplings vanish when the potential curves are proportional to $1/R^2$. Therefore, the system is described by a set of uncoupled one-dimensional Schrödinger equations that can be solved analytically once the trapping potential is included. These procedures lead to simple expressions for the trapped energies [57]

$$E_{\nu n} = (p_\nu + 2n + 5/2)\hbar\omega, \tag{35}$$

where ω is the trapping frequency and we have included the zero-point energy of the center-of-mass motion. In Ref. [38], the $2\hbar\omega$ spacing was verified and the lowest p_ν coefficients were identified. Equations (34) and (35) are also valid in the noninteracting limit. For $L=0$ and positive-parity solutions, the p_ν^{NI} values and their degeneracies λ_ν have relatively simple closed forms: $p_\nu^{NI}=11/2+2\nu$ and $\lambda_\nu=\nu^4/96+7\nu^3/48+17\nu^2/24+133\nu/96+57/64+(-1)^\nu\nu/32+7/64(-1)^\nu$. Their lowest values can be found in Table I.

The development of the CGHS method allows us to carry out a hyperspherical calculation for the four-fermion problem and to directly verify the form of the hyperspherical potentials. Also, it allows us to analyze deviations from the zero-range solutions due to finite-range effects.

The 20 lowest four-body potential curves $2\mu R^2 U_\nu(R)/\hbar^2$ for the equal-mass system are presented in Fig. 2. We can identify three regimes in these potential curves. The region $R \lesssim r_0$ is controlled by the kinetic energy. The kinetic-energy effects are more important than the interaction energy and the potential curves are well approximated by the noninteracting potential curves. In other words, $2\mu R^2 U_\nu(R)/\hbar^2 \approx (p_\nu^{NI})^2 - 1/4$ and the eigenchannels are well approximated by the hyperspherical harmonics (see Sec. II B). For that reason, there is a large degeneracy in the $R \lesssim r_0$ region which corresponds to the degeneracy of the Λ^2 operator. Furthermore, the potential curves are, to a good approximation, proportional to $1/R^2$. The second region is $r_0 \lesssim R \lesssim 20 r_0$. In this region, both the kinetic and the interaction terms are important and finite-range effects are important. In the third region, $R \gtrsim 20 r_0$, the potential curves recover their universal behavior. The potential curves are, again, approximately proportional to $1/R^2$. As R/r_0 increases, finite-range effects tend to zero and we obtain the zero-range potential curves at unitarity. Therefore, in this region, the eigenvalues of $2\mu R^2 U_\nu(R)/\hbar^2$ are approximately $(p_\nu^2 - 1/4)$. Thus, we can compare these results to the ones deduced from trapped calculations for $r_0/a_{ho}=0.01$ presented in Ref. [38]. The solid lines correspond to $(p_0^2-1/4)$, $(p_1^2-1/4)$, and $(p_2^2-1/4)$, respectively [75]. There is good agreement between the predictions from the trapped system obtained with CG and the direct computation of the potential curves through CGHS.

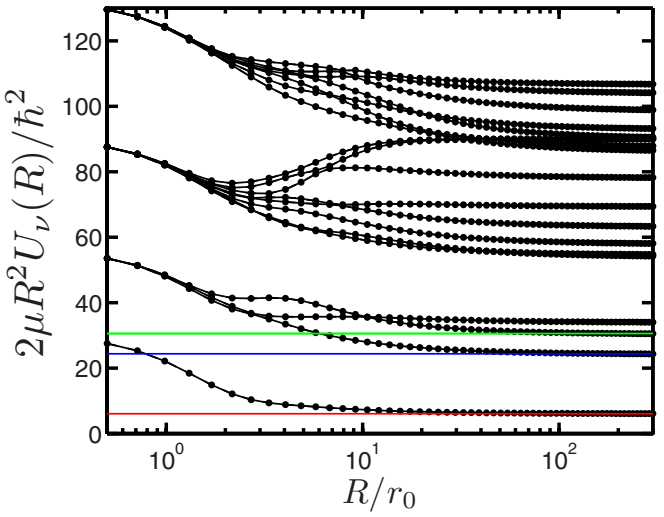

FIG. 2. (Color online) Hyperspherical potential curves at unitarity $(a \to \infty)$ for the four-fermion system multiplied by $2\mu R^2/\hbar^2$. Solid lines represent the predictions from analyzing the spectrum obtained with the CG method. The symbols correspond to direct evaluation of the potential curves with the CGHS method.

To quantify this last statement, we analyze the value of p_0. Several groups [23,58–61] tried to benchmark the four-body value of E_{00}, which is simply related to p_0. The calculations from Ref. [60] use zero-range interactions explicitly and they report a value of $E_{00} \approx (5.045 \pm 0.003)\hbar\omega$. To extract the p_0 value in the zero-range limit, we carry out two different calculations. First, we study the E_{00} energy obtained with the standard CG method as a function of the range of the two-body interaction and then we extrapolate to zero-range limit. This method was previously applied for the three-body system and the numerical results agreed with the analytical predictions up to seven digits [40]. The same procedure applied to the four-body system leads to $p_0 \approx 2.5096$. The second calculation analyzes the long-range behavior of the potential curves. To eliminate finite-range effects, we extrapolate the potential curve $U_0(R)$ to $R/r_0 \to \infty$. In this limit, $U_0(R)$ is characterized by a value $p_0 \approx 2.5092$. These two different methods provide a value of p_0 which agrees in four digits. These values are slightly lower than $p_0 \approx 2.545 \pm 0.003$ predicted in Ref. [60]. This suggests that the uncertainty in Ref. [60] was apparently underestimated.

TABLE II. Coefficients p_ν of the four-fermion potential curves.

ν	p_ν	ν	p_ν	ν	p_ν
0	2.509	7	7.959	14	9.502
1	4.944	8	8.341	15	9.648
2	5.529	9	8.848	16	9.938
3	5.846	10	9.292	17	10.205
4	7.363	11	9.366	18	10.339
5	7.402	12	9.5	19	10.482
6	7.621	13	9.501		

The calculations of the lowest 20 universal coefficients p_ν are reported in Table II. It is interesting to note that some of the p_ν coefficients are very similar to the noninteracting coefficients. For example, the p_ν coefficients for $\nu=12$, 13, and 14 coincide with noninteracting p_ν^{NI} coefficient. Two of these potential curves are also described by $p_\nu=9.5$ in the small R region and deviate from these values in the region $R\sim r_0$. These channels have nodes in every spin-up–spin-down interparticle distance, therefore at large distances, they recover the noninteracting behavior. The third potential curve smoothly decreases from $p_\nu^{NI}=11.5$ at small R to $p_\nu=9.5$ at large R.

Finally, note that the CGHS method has been successfully applied to the four-boson system [72,73,76]. In that study, the four-boson spectrum is calculated from the CGHS potential curves. Also, that study considered scattering events such as four-body recombination, which was calculated and predicted to be important for the understanding of a recent experiment on Efimov physics in an ultracold Bose gas [4].

V. CONCLUSIONS

We have presented a numerical method suitable for the analysis of four-body processes. We have shown several examples for three- and four-particle systems recovering known results. Furthermore, we have obtained the lowest 20 p_ν coefficients for the two-component four-fermion system that characterize both free and trapped systems. These coefficients also characterize the spectrum of four trapped fermions at unitarity. Our results considerably extend previous calculations and provide more accurate energies.

The CGHS method has been used to analyze the four-boson system in Refs. [72,73,76], predicting unique phenomena observed experimentally [77]. It has also built a theoretical foundation for the analysis of four-body collisional processes in other systems such as two-component Bose systems [78–81], Bose-Fermi mixtures [82–84], and three-component Fermi gases [85–87]. Even though this method was initially implemented to treat ultracold systems using model potentials, it can be in principle extended to other four-body problems.

ACKNOWLEDGMENTS

The authors would like to thank S. T. Rittenhouse, N. P. Mehta, and J. P. D'Incao for useful discussions and for providing their four-fermion numerical data (dashed curves included in Fig. 1). This work was supported in part by NSF.

APPENDIX A: APPLICATION OF CORRELATED GAUSSIANS TO THE HYPERSPHERICAL FRAMEWORK

This appendix illustrates how correlated Gaussian basis functions can be used in the general hyperspherical framework presented in Sec. II C. First, we consider the three-particle case and calculate the matrix elements [Eqs. (21), (22), and (29)]. Then, we discuss how to generate and optimize the basis set.

1. Unsymmetrized matrix-element evaluation for three particles

In this section, we present as an example the evaluation of the matrix elements [Eqs. (21), (22), and (29)] of three-particle system. Consider a system in which the center-of-mass motion decouples. Then, the $L^P=0^+$ solutions of the body-fixed system can be expanded in terms of the interparticle distances. For the three-body system, the correlated basis functions take the form

$$\Psi_A(r_{12},r_{13},r_{23})=\exp\left[-\left(\frac{r_{12}^2}{2d_{12}^2}+\frac{r_{13}^2}{2d_{13}^2}+\frac{r_{23}^2}{2d_{23}^2}\right)\right]. \tag{A1}$$

For equal-mass systems, we can write Eq. (A1) in terms of the following Jacobi coordinates:

$$\mathbf{x}_1=\frac{1}{\sqrt{2}}(\mathbf{r}_1-\mathbf{r}_2), \tag{A2}$$

$$\mathbf{x}_2=\sqrt{\frac{2}{3}}\left(\mathbf{r}_3-\frac{\mathbf{r}_1+\mathbf{r}_2}{2}\right). \tag{A3}$$

The basis functions [Eq. (A1)] can be written as

$$\begin{aligned}\Psi_A(r_{12},r_{13},r_{23})&=\langle \mathbf{x}_1,\mathbf{x}_2|A\rangle\\&=\exp\left(-\frac{\mathbf{x}^T\cdot A\cdot\mathbf{x}}{2}\right)\\&=\exp\left(-\frac{\mathbf{x}_1\cdot\mathbf{x}_1a_{11}+2\mathbf{x}_1\cdot\mathbf{x}_2a_{12}+\mathbf{x}_2\cdot\mathbf{x}_2a_{22}}{2}\right),\end{aligned} \tag{A4}$$

where $\mathbf{x}\equiv\{\mathbf{x}_1,\mathbf{x}_2\}$ and A is a 2 by 2 symmetric matrix whose elements are $a_{11}=2/d_{12}^2+1/2(1/d_{13}^2+1/d_{23}^2)$, $a_{12}=a_{21}=\sqrt{3}/2(1/d_{23}^2-1/d_{13}^2)$, and $a_{22}=3/2(1/d_{13}^2+1/d_{23}^2)$. In Eq. (A4), we can clearly see that the state $\langle \mathbf{x}_1,\mathbf{x}_2|A\rangle$ depends only on the distances x_1 and x_2 plus the angle θ_{12} between them, $\cos\theta_{12}=\mathbf{x}_1\cdot\mathbf{x}_2/x_1x_2$.

We want to obtain the matrix elements corresponding to these basis functions at fixed hyperradius R. We define the hyperradius to be $R^2=\mathbf{x}_1^2+\mathbf{x}_2^2$. The integrand of the overlap matrix element between $|A\rangle$ and $|B\rangle$, noted as BA, is

$$BA = \exp\left(-\frac{\mathbf{x}^T\cdot(A+B)\cdot\mathbf{x}}{2}\right). \tag{A5}$$

We change to the Jacobi basis set that diagonalizes $A+B$ and we call β_1 and β_2 the eigenvalues and $\mathbf{y}\equiv\{\mathbf{y}_1,\mathbf{y}_2\}$ the orthonormal eigenvectors. In this new coordinate basis, Eq. (A5) has a simple form

$$BA = \exp\left(-\frac{\beta_1 y_1^2+\beta_2 y_2^2}{2}\right). \tag{A6}$$

We integrate over the angles of the vectors $\mathbf{y}_1$ and $\mathbf{y}_2$ and we fix the hyperradius, so $y_1=R\cos\theta$ and $y_2=R\sin\theta$. In this set of coordinates, the matrix element at fixed R is

$$\langle B|A\rangle|_R = (4\pi)^2\int_0^{\pi/2} e^{-R^2(\beta_1\cos^2\theta+\beta_2\sin^2\theta)/2}\cos^2\theta\sin^2\theta d\theta. \tag{A7}$$

This integration has a closed-form result

$$\langle B|A\rangle|_R = 2\pi^3\frac{\exp\left(-\frac{\beta_1+\beta_2}{4}R^2\right)}{\xi}I_1(\xi). \tag{A8}$$

Here we have introduced the definition $\xi=R^2(\beta_1-\beta_2)/4$.

To simplify the interaction matrix-element evaluation, we can adopt a Gaussian model potential as was utilized in the CG method. In this case, the interaction term can be evaluated in the same way we have calculated the overlap term since the interaction is also a Gaussian. Each pairwise interaction can be easily written as $V_{ij}=V_0\exp(-\frac{r_{ij}^2}{2r_0^2})=V_0\exp[-\mathbf{x}^T\cdot M^{(ij)}\cdot\mathbf{x}/(2r_0^2)]$. Therefore, to calculate the interaction matrix element, we need to evaluate

$$\langle B|V_{ij}|A\rangle = V_0\int d\Omega\,\exp\left(-\frac{\mathbf{x}^T\cdot(A+B+M^{(ij)}/r_0^2)\cdot\mathbf{x}}{2}\right). \tag{A9}$$

This integration can be done following the same steps of the overlap matrix element. Equation (A8) can be used directly if we multiply it by V_0, and β_1 and β_2 are replaced by the eigenvalues of $A+B+M^{(ij)}/r_0^2$. Note that for each pairwise interaction (and for each pair of basis functions in the matrix element), the matrix $M^{(ij)}$ changes and requires a new evaluation of the eigenvalues.

The third term we need to evaluate is the hyperangular kinetic term at fixed R. This kinetic term is proportional to the grand angular-momentum operator Λ defined for the $N_P=3$ case as

$$\frac{\Lambda^2\hbar^2}{2\mu R^2} = -\sum_i\frac{\hbar^2\nabla_i^2}{2\mu}+\frac{\hbar^2}{2\mu}\frac{1}{R^5}\frac{\partial}{\partial R}R^5\frac{\partial}{\partial R}. \tag{A10}$$

The expression can be formally written as

$$\mathcal{T}_\Omega = \mathcal{T}_T-\mathcal{T}_R, \tag{A11}$$

where

$$\mathcal{T}_\Omega = \frac{\Lambda^2\hbar^2}{2\mu R^2},\quad \mathcal{T}_T = -\sum_i\frac{\hbar^2\nabla_i^2}{2\mu} \tag{A12}$$

and

$$\mathcal{T}_R = -\frac{\hbar^2}{2\mu}\frac{1}{R^5}\frac{\partial}{\partial R}R^5\frac{\partial}{\partial R}. \tag{A13}$$

In typical calculations, $\mathcal{T}_\Omega$ is evaluated by directly applying the corresponding derivatives in the hyperangles Ω. However, in this case, it is convenient to evaluate $\mathcal{T}_T$ and $\mathcal{T}_R$ separately and make use of Eq. (A11).

The integrand of the total kinetic term $\mathcal{T}_T$ takes the form

$$B|\mathcal{T}_T|A = \exp\left(-\frac{\mathbf{x}^T\cdot B\cdot\mathbf{x}}{2}\right)\left(-\sum_i^2\frac{\hbar^2}{2\mu}\nabla_i^2\right)\exp\left(-\frac{\mathbf{x}^T\cdot A\cdot\mathbf{x}}{2}\right). \tag{A14}$$

First, we diagonalize A and use the eigenvectors and eigenvalues of A, obtaining

$$B|\mathcal{T}_T|A = -\frac{\hbar^2}{2\mu}(-\mathrm{Tr}[A]+\mathbf{x}^T\cdot A^2\cdot\mathbf{x})\exp\left(-\frac{\mathbf{x}^T\cdot(A+B)\cdot\mathbf{x}}{2}\right). \tag{A15}$$

Here Tr is the trace function. We can use $\mathrm{Tr}[A]=(\alpha_1+\alpha_2)$, where α_1 and α_2 are the eigenvalues of A. Now we diagonalize $A+B$. We call T the matrix with the orthonormal eigenstates in columns, and β_1 and β_2 are the eigenvalues of $A+B$. We make a change of coordinates to the basis set that diagonalizes $A+B$. We obtain

$$B|\mathcal{T}_T|A = -\frac{\hbar^2}{2\mu}[-3(\alpha_1+\alpha_2)+\mathbf{y}\cdot G\cdot\mathbf{y}]\exp\left(-\frac{\beta_1 y_1^2+\beta_2 y_2^2}{2}\right), \tag{A16}$$

where $G=T^TA^2T$, and $\mathbf{y}_1$ and $\mathbf{y}_2$ are the vectors in the new eigenbasis. The integration over the angles of these vectors is trivial. After this integration, we fix the hyperradius and integrate over the hyperangle θ defined by $y_1=R\cos\theta$ and $y_2=R\sin\theta$,

$$\begin{aligned}\langle B|\mathcal{T}_T|A\rangle|_R = -\frac{(4\pi)^2\hbar^2}{2\mu}\int_0^{\pi/2}&[-3(\alpha_1+\alpha_2)+g_{11}R^2\\&\times\cos^2\theta+g_{22}R^2\sin^2\theta]\\&\times\exp\left(-\frac{\beta_1R^2\cos^2\theta+\beta_2R^2\sin^2\theta}{2}\right)\\&\times\cos^2\theta\sin^2\theta d\theta.\end{aligned} \tag{A17}$$

This integration can be done analytically and the results expressed in terms of the Bessel functions I_1 and I_0,

$$\begin{aligned}\langle B|\mathcal{T}_T|A\rangle|_R = -\frac{\hbar^2e^{-(\beta_1+\beta_2)R^2/2}\pi^3R^2}{16\xi\mu}&\Bigg\{-8(g_{11}-g_{22})I_0[\xi]\\&+\frac{2}{\xi}\{8(g_{11}-g_{22})+(\beta_1-\beta_2)[-6(\alpha_1+\alpha_2)\\&+(g_{11}+g_{22})R^2]\}I_1[\xi]\Bigg\}.\end{aligned} \tag{A18}$$

Now we will evaluate $\mathcal{T}_R$, the hyperradial kinetic term. It is written as

$$\mathcal{T}_R = -\frac{\hbar^2}{2\mu}\left(\frac{1}{R^{5/2}}\frac{\partial^2}{\partial R^2}R^{5/2} - \frac{15}{4R^2}\right). \tag{A19}$$

Therefore, the integrand takes the form

$$B|\mathcal{T}_R|A = -\frac{\hbar^2}{2\mu}\exp\left(-\frac{\mathbf{x}^T\cdot B\cdot\mathbf{x}}{2}\right)\left(\frac{1}{R^{5/2}}\frac{\partial^2}{\partial R^2}R^{5/2} - \frac{15}{4R^2}\right) \times\exp\left(-\frac{\mathbf{x}^T\cdot A\cdot\mathbf{x}}{2}\right). \tag{A20}$$

We use the property $\mathbf{x}^T\cdot A\cdot\mathbf{x}=R^2F_A(\Omega)$ to evaluate the derivatives with respect to R. This allows a simple calculation of the derivatives in Eq. (A20), yielding

$$B|\mathcal{T}_R|A = \frac{\hbar^2}{2\mu R^2}[6\mathbf{x}^T\cdot A\cdot\mathbf{x} - (\mathbf{x}^T\cdot A\cdot\mathbf{x})^2]e^{-\mathbf{x}^T\cdot(A+B)\cdot\mathbf{x}/2}. \tag{A21}$$

Next we diagonalize $A+B$ and set $D=T^TAT$ giving

$$B|\mathcal{T}_R|A = \frac{\hbar^2}{2\mu R^2}[6\mathbf{y}\cdot D\cdot\mathbf{y} - (\mathbf{y}\cdot D\cdot\mathbf{y})^2]\exp\left(-\frac{\beta_1 y_1^2+\beta_2 y_2^2}{2}\right). \tag{A22}$$

The terms $\mathbf{y}\cdot D\cdot\mathbf{y}$ and $(\mathbf{y}\cdot D\cdot\mathbf{y})^2$ depend on the polar angles of the vectors. The integration over the polar angles ($\Omega_1=\{\phi_1,\theta_1\}$ and $\Omega_2=\{\phi_2,\theta_2\}$) of these terms is

$$\int[6\mathbf{y}\cdot D\cdot\mathbf{y} - (\mathbf{y}\cdot D\cdot\mathbf{y})^2]d\Omega_1 d\Omega_2 = (4\pi)^2\{6d_{11}y_1^2 + 6d_{22}y_2^2 - [d_{11}^2y_1^4 + (2d_{11}d_{22}+4d_{12}^2/3)y_1^2y_2^2 + d_{22}^2y_2^4]\}. \tag{A23}$$

Now we carry out the integration over the hyperangle θ, using $y_1=R\cos\theta$ and $y_2=R\sin\theta$, which gives

$$\langle B|\mathcal{T}_R|A\rangle|_R = \frac{(4\pi)^2\hbar^2}{2\mu R^2}\int_0^{\pi/2}\{6d_{11}R^2\cos^2\theta + 6d_{22}R^2\sin^2\theta - d_{11}^2R^4\cos^4\theta - (2d_{11}d_{22} + 4d_{12}^2/3)R^4\cos^2\theta\sin^2\theta - d_{22}^2R^4 \times\sin^4\theta\}\exp\left(-\frac{\beta_1R^2\cos^2\theta+\beta_2R^2\sin^2\theta}{2}\right) \times\cos^2\theta\sin^2\theta d\theta. \tag{A24}$$

This integration has the analytical form

$$\langle B|\mathcal{T}_R|A\rangle|_R = -\frac{\hbar^2}{\mu}\frac{e^{-(\beta_1+\beta_2)R^2/4}\pi^3R^2}{64\xi^2}\left\{-8\{-8d_{12}^2 + (d_{11}-d_{22}) \times[6(-\beta_1+\beta_2+d_{11}-d_{22}) + 4\xi(d_{11}+d_{22})]\}I_0[\xi] + \frac{2}{\xi}[-64d_{12}^2 + 48(d_{11}-d_{22})(-\beta_1+\beta_2+d_{11} - d_{22}) + 8\xi(-3\beta_1+3\beta_2+4d_{11}-4d_{22}) \times(d_{11}+d_{22}) + 16\xi^2(d_{11}^2+d_{22}^2)]I_1[\xi]\right\}. \tag{A25}$$

Combining Eqs. (A18) and (A25), we obtain $\mathcal{T}_\Omega$. The expression for $\mathcal{T}_\Omega$ can be simplified using the relation $G=D^2$ to write G matrix elements of Eq. (A18) in terms of the ones of D. This same procedure can be applied to extract the P and $\tilde{Q}$ matrix elements

$$\left\langle B|\frac{\partial A}{\partial R}\right\rangle\Big|_R \quad\text{and}\quad \left\langle\frac{\partial B}{\partial R}|\frac{\partial A}{\partial R}\right\rangle\Big|_R. \tag{A26}$$

A useful test to verify the functional form of the matrix elements is to integrate them with respect to R, with the corresponding volume element, and compare that result to the standard CG matrix elements. Another important test is to verify that $\mathcal{T}_\Omega$ is symmetric under the exchange of the basis functions A and B. This is not a trivial test since neither $\mathcal{T}_T$ nor $\mathcal{T}_R$ is symmetric.

A major advantage of these matrix-element evaluations is that they can be easily extended to four particles. In general, these matrix-element evaluations would require a 5D numerical integration but for these basis functions, with the above analytical development, they only require a 1D numerical integration.

2. General considerations

Many of the procedures of the standard CG method can be easily extended to the CGHS. The selection, symmetrization, and optimization of a basis follow the same ideas of the standard CG method. However, the evaluation of the unsymmetrized matrix elements at fixed R is clearly different. Furthermore, the hyperangular Hamiltonian [Eq. (17)] needs to be solved at different hyperradius R.

There are several properties that make this method particularly efficient. For the model potential used, the scattering length is tuned by varying the potential depths of the two-body interaction. Therefore, as in the CG case, the matrix elements need only be calculated once; then they can be used for a wide range of scattering lengths. Of course, the basis set should be complete enough to describe the relevant potential curves at all the desired scattering length values.

The selection of the basis function generally depends on R. To avoid numerical problems, the mean hyperradius of each basis function $\langle R\rangle_B$ should be comparable to the hyperradius R in which the matrix elements are evaluated. We can ensure that $\langle R\rangle_B\sim R$ by selecting some (or all) of the weights d_{ij} to be of the order of R.

We consider two different optimization procedures. The first possible optimization procedure is the following. First, we select a few basis functions and optimize them to describe the lowest hyperspherical harmonics. The Gaussian widths of these basis functions are rescaled by R at each hyperradius so that they represent the hyperspherical harmonics equally well. These basis functions are used at all R, while the remaining are optimized at each R. Starting from small R (of the order of the range of the potential), we optimize a set of basis functions. As R is increased, the basis set is increased and reoptimized. At every R step, only a fraction

of the basis set is optimized and those basis functions are selected randomly. After several R steps, the basis set is increased.

Instead of optimizing the basis set at each R, one can alternatively try to create a complete basis set at large $R_{\max}$. In this case, the basis functions should be complete enough to describe the lowest channel functions with interparticle distances varying from interaction range r_0 up to the hyperradius $R_{\max}$. Such a basis set can be rescaled to any $R < R_{\max}$ and should efficiently describe the channel functions at that R. The rescaling procedure is simply $d_{ij}/R = d_{ij}^{\max}/R_{\max}$. This procedure avoids the optimization at each R. Furthermore, the kinetic, overlap, and coupling matrix elements at R are straightforwardly related with the ones at $R_{\max}$. So, the interaction potential is the only matrix element that needs to be recalculated at each R. This property can be understood using dimensional analysis. The kinetic, overlap, and coupling matrix elements only depend on R, so a rescaling of the widths is simply related to a rescaling of the matrix elements. In contrast, the interaction potential introduces a new length scale, so the matrix elements depend on both R and r_0, and the rescaling does not work.

These two methods, the "complete basis set" and the "small optimized basis set" methods, can be appropriate in different circumstances. If a large number of channels is needed, probably the complete basis method is the better choice. But, if only a couple of particular channel potential curves and couplings are needed, then the small optimized basis set method might be more efficient.

The most convenient strategy we have found for optimizing the basis function in the four-boson and four-fermion problems is the following. First we select an hyperradius R_m that is $R_m \approx 300 r_0$ where the basis function will be initially optimized. The basis set is increased and optimized until the relevant potential curves are converged and, in that sense, the basis is complete. This basis is then rescaled, as proposed in the second optimization method, to all $R < R_m$. For $R > R_m$, it is too expensive to have a "complete" basis set. For that reason, we use the small optimized basis set method which allows a reliable description of the lowest potential curves.

Note that for standard correlated Gaussian calculations, the matrices A and B need to be positive definite. This condition restricts the Hilbert space to exponentially decaying functions. In the hyperspherical treatment, this is not necessary since the matrix elements can always be calculated at fixed R as the integrals converge even for exponentially growing functions. This gives more flexibility in choosing the optimal basis functions.

[1] E. Braaten and H. W. Hammer, Phys. Rep. **428**, 259 (2006).
[2] V. Efimov, Yad. Fiz. **12**, 1080 (1970) [Sov. J. Nucl. Phys. **12**, 589 (1971)].
[3] B. D. Esry, C. H. Greene, and J. P. Burke, Jr., Phys. Rev. Lett. **83**, 1751 (1999).
[4] T. Kraemer *et al.*, Nature (London) **440**, 315 (2006).
[5] D. M. Eagles, Phys. Rev. **186**, 456 (1969).
[6] A. J. Leggett, in *Modern Trends in the Theory of Condensed Matter*, edited by A. Pekalski and J. Przystawa (Springer, Berlin, 1980).
[7] P. Nozières and S. Schmitt-Rink, J. Low Temp. Phys. **59**, 195 (1985).
[8] M. Greiner, C. A. Regal, and D. S. Jin, Nature (London) **426**, 537 (2003).
[9] S. Jochim, M. Bartenstein, A. Altmeyer, G. Hendl, S. Riedl, C. Chin, J. Hecker Denschlag, and R. Grimm, Science **302**, 2101 (2003).
[10] M. W. Zwierlein, C. A. Stan, C. H. Schunck, S. M. F. Raupach, S. Gupta, Z. Hadzibabic, and W. Ketterle, Phys. Rev. Lett. **91**, 250401 (2003).
[11] T. Bourdel, L. Khaykovich, J. Cubizolles, J. Zhang, F. Chevy, M. Teichmann, L. Tarruell, S. J. J. M. F. Kokkelmans, and C. Salomon, Phys. Rev. Lett. **93**, 050401 (2004).
[12] C. A. Regal, M. Greiner, and D. S. Jin, Phys. Rev. Lett. **92**, 040403 (2004).
[13] M. W. Zwierlein, C. A. Stan, C. H. Schunck, S. M. F. Raupach, A. J. Kerman, and W. Ketterle, Phys. Rev. Lett. **92**, 120403 (2004).
[14] M. W. Zwierlein, J. R. Abo-Shaeer, A. Schirotzek, C. H. Schunck, and W. Ketterle, Nature (London) **435**, 1047 (2005).
[15] D. Jaksch, C. Bruder, J. I. Cirac, C. W. Gardiner, and P. Zoller, Phys. Rev. Lett. **81**, 3108 (1998).
[16] B. Paredes, A. Widera, V. Murg, O. Mandel, S. Fölling, I. Cirac, G. Shlyapnikov, T. Hänsch, I. Bloch, and N. Contact, Nature (London) **429**, 277 (2004).
[17] T. Kinoshita, T. Wenger, and D. Weiss, Science **305**, 1125 (2004).
[18] I. Bloch, J. Dalibard, and W. Zwerger, Rev. Mod. Phys. **80**, 885 (2008).
[19] D. S. Petrov, Phys. Rev. Lett. **93**, 143201 (2004).
[20] D. S. Petrov, Phys. Rev. A **67**, 010703(R) (2003).
[21] D. S. Petrov, C. Salomon, and G. V. Shlyapnikov, Phys. Rev. Lett. **93**, 090404 (2004).
[22] A. Deltuva and A. Fonseca, Phys. Rev. Lett. **98**, 162502 (2007).
[23] J. von Stecher and C. H. Greene, Phys. Rev. Lett. **99**, 090402 (2007).
[24] J. P. D'Incao, S. T. Rittenhouse, N. P. Mehta, and C. H. Greene, Phys. Rev. A **79**, 030501(R) (2009).
[25] Y. Wang and B. D. Esry, Phys. Rev. Lett. **102**, 133201 (2009).
[26] L. D. Faddeev, Zh. Eksp. Teor. Fiz. **39**, 1459 (1960).
[27] Y. Suzuki and K. Varga, *Stochastic Variational Approach to Quantum-Mechanical Few-Body Problems* (Springer-Verlag, Berlin, 1998).
[28] R. A. Malfliet and J. A. Tjon, Nucl. Phys. A. **127**, 161 (1969).
[29] O. A. Yakubovsky, Yad. Fiz. **5**, 1312 (1967) [Sov. J. Nucl. Phys. **5**, 937 (1967)].
[30] J. Macek, J. Phys. B **1**, 831 (1968).
[31] K. Singer, Proc. R. Soc. London, Ser. A **258**, 412 (1960).
[32] S. F. Boys, Proc. R. Soc. London, Ser. A **258**, 402 (1960).
[33] V. I. Kukulin and V. Krasnopol'sky, J. Phys. G **3**, 795 (1977).
[34] K. Varga and Y. Suzuki, Phys. Rev. A **53**, 1907 (1996).
[35] K. Varga and Y. Suzuki, Phys. Rev. C **52**, 2885 (1995).
[36] K. Varga and Y. Suzuki, Comput. Phys. Commun. **106**, 157

(1997).
[37] K. Varga, Y. Suzuki, and R. G. Lovas, Nucl. Phys. A. **571**, 447 (1994).
[38] D. Blume, J. von Stecher, and C. H. Greene, Phys. Rev. Lett. **99**, 233201 (2007).
[39] J. von Stecher and C. H. Greene, Phys. Rev. A **75**, 022716 (2007).
[40] J. von Stecher, C. H. Greene, and D. Blume, Phys. Rev. A **77**, 043619 (2008).
[41] J. Mezei, A. Kruppa, and K. Varga, Few-Body Syst. **41**, 233 (2007).
[42] J. Y. Zhang, J. Mitroy, and K. Varga, Phys. Rev. A **78**, 042705 (2008).
[43] K. Varga, J. Mitroy, J. Z. Mezei, and A. T. Kruppa, Phys. Rev. A **77**, 044502 (2008).
[44] J. Mitroy, J. Y. Zhang, and K. Varga, Phys. Rev. Lett. **101**, 123201 (2008).
[45] L. M. Delves, Nucl. Phys. **9**, 391 (1959).
[46] L. M. Delves, Nucl. Phys. **20**, 275 (1960).
[47] C. D. Lin, Phys. Rep. **257**, 1 (1995).
[48] Y. F. Smirnov and K. V. Shitikova, Sov. J. Part. Nucl. **8**, 44 (1977).
[49] X. Chapuisat, Phys. Rev. A **45**, 4277 (1992).
[50] M. Aymar, C. H. Greene, and E. Luc-Koenig, Rev. Mod. Phys. **68**, 1015 (1996).
[51] O. Zatsarinny and K. Bartschat, J. Phys. B **37**, 2173 (2004).
[52] A. Sunderland, C. Noble, V. Burke, and P. Burke, Comput. Phys. Commun. **145**, 311 (2002).
[53] R. T. Pack and G. A. Parker, J. Chem. Phys. **87**, 3888 (1987).
[54] Y. Zhou, C. D. Lin, and J. Shertzer, J. Phys. B **26**, 3937 (1993).
[55] B. D. Esry, C. D. Lin, and C. H. Greene, Phys. Rev. A **54**, 394 (1996).
[56] H. Suno, B. D. Esry, C. H. Greene, and J. P. Burke, Jr., Phys. Rev. A **65**, 042725 (2002).
[57] F. Werner and Y. Castin, Phys. Rev. A **74**, 053604 (2006).
[58] S. Y. Chang and G. F. Bertsch, Phys. Rev. A **76**, 021603(R) (2007).
[59] J. von Stecher, C. H. Greene, and D. Blume, Phys. Rev. A **76**, 053613 (2007).
[60] Y. Alhassid, G. F. Bertsch, and L. Fang, Phys. Rev. Lett. **100**, 230401 (2008).
[61] I. Stetcu, B. R. Barrett, U. van Kolck, and J. P. Vary, Phys. Rev. A **76**, 063613 (2007).
[62] H. H. Sørensen, D. V. Fedorov, and A. S. Jensen, AIP Conf. Proc. **777**, 12 (2005).
[63] H. H. Sørensen, M.S. thesis, University of Aarhus, 2005 [e-print arXiv:cond-mat/0502126].
[64] U. Fano, Phys. Rev. A **24**, 2402 (1981).
[65] Even though μ is arbitrary, there is one preferable selection $\mu=[\Pi_i m_i/(\Sigma_i m_i)]^{1/(N-1)}$ that conserves the volume element of the coordinate transformation [46]. In this paper, we will only present results for equal-mass systems for which it is simpler to simply choose $\mu=m$.
[66] H. T. Coelho and J. E. Hornos, Phys. Rev. A **43**, 6379 (1991).
[67] N. P. Mehta, S. T. Rittenhouse, J. P. D'Incao, and C. H. Greene, e-print arXiv:0706.1296.
[68] The $(3N_P\text{-}7)$ numerical integration results from the following reasoning: initially, we have $3N_P$ numerical integration but three dimensions are removed by decoupling the center of mass motion, three dimensions are removed fixing the Euler angles, and one dimension is removed by fixing R.
[69] J. von Stecher, Ph.D. thesis, University of Colorado, 2008; available at http://jilawww.colorado.edu/pubs/thesis/vonstecher/vonstecherthesis.pdf.
[70] J. Macek, Z. Phys. D: At., Mol. Clusters **3**, 31 (1986).
[71] D. Blume and C. H. Greene, J. Chem. Phys. **112**, 8053 (2000).
[72] J. von Stecher, J. P. D'Incao, and C. H. Greene, Nat. Phys. **5**, 417 (2009).
[73] J. P. D'Incao, J. von Stecher, and C. H. Greene, Phys. Rev. Lett. **103**, 033004 (2009).
[74] S. Tan, e-print arXiv:cond-mat/0412764.
[75] The coefficients p_ν can be easily related with the s_ν of Ref. [38] by $s_\nu=p_{\nu-1}-1/2$.
[76] N. P. Mehta, S. T. Rittenhouse, J. P. D'Incao, J. von Stecher, and C. H. Greene, e-print arXiv:0903.4145.
[77] F. Ferlaino, S. Knoop, M. Berninger, W. Harm, J. P. D'Incao, H. C. Nägerl, and R. Grimm, Phys. Rev. Lett. **102**, 140401 (2009).
[78] S. B. Papp, J. M. Pino, and C. E. Wieman, Phys. Rev. Lett. **101**, 040402 (2008).
[79] C. J. Myatt, E. A. Burt, R. W. Ghrist, E. A. Cornell, and C. E. Wieman, Phys. Rev. Lett. **78**, 586 (1997).
[80] G. Thalhammer, G. Barontini, L. De Sarlo, J. Catani, F. Minardi, and M. Inguscio, Phys. Rev. Lett. **100**, 210402 (2008).
[81] C. Weber, G. Barontini, J. Catani, G. Thalhammer, M. Inguscio, and F. Minardi, Phys. Rev. A **78**, 061601(R) (2008).
[82] G. Modugno, G. Roati, F. Riboli, F. Ferlaino, R. Brecha, and M. Inguscio, Science **297**, 2240 (2002).
[83] S. Inouye, J. Goldwin, M. L. Olsen, C. Ticknor, J. L. Bohn, and D. S. Jin, Phys. Rev. Lett. **93**, 183201 (2004).
[84] M. L. Olsen, J. D. Perreault, T. D. Cumby, and D. S. Jin, e-print arXiv:0810.1965.
[85] T. B. Ottenstein, T. Lompe, M. Kohnen, A. N. Wenz, and S. Jochim, Phys. Rev. Lett. **101**, 203202 (2008).
[86] J. H. Huckans, J. R. Williams, E. L. Hazlett, R. W. Stites, and K. M. O'Hara, Phys. Rev. Lett. **102**, 165302 (2009).
[87] D. Blume, S. T. Rittenhouse, J. von Stecher, and C. H. Greene, Phys. Rev. A **77**, 033627 (2008).